doi:10.1093/brain/awz365 BRAIN 2020: 143; 161–174 | 161

BRAIN
A JOURNAL OF NEUROLOGY

Adult loss of *Cacna1a* in mice recapitulates childhood absence epilepsy by distinct thalamic bursting mechanisms

Qing-Long Miao,[1] Stefan Herlitze,[2] Melanie D. Mark[2] and Jeffrey L. Noebels[1,3,4]

Inborn errors of *CACNA1A*-encoded P/Q-type calcium channels impair synaptic transmission, producing early and lifelong neurological deficits, including childhood absence epilepsy, ataxia and dystonia. Whether these impairments owe their pathologies to defective channel function during the critical period for thalamic network stabilization in immature brain remains unclear. Here we show that mice with tamoxifen-induced adult-onset ablation of P/Q channel alpha subunit ($iKO^{p/q}$) display identical patterns of dysfunction, replicating the inborn loss-of-function phenotypes and, therefore demonstrate that these neurological defects do not rely upon developmental abnormality. Unexpectedly, unlike the inborn model, the adult-onset pattern of excitability changes believed to be pathogenic within the thalamic network is non-canonical. Specifically, adult ablation of P/Q channels does not promote *Cacna1g*-mediated burst firing or T-type calcium current (I_T) in the thalamocortical relay neurons; however, burst firing in thalamocortical relay neurons remains essential as $iKO^{p/q}$ mice generated on a *Cacna1g* deleted background show substantially diminished seizure generation. Moreover, in thalamic reticular nucleus neurons, burst firing is impaired accompanied by attenuated I_T. Interestingly, inborn deletion of thalamic reticular nucleus-enriched, human childhood absence epilepsy-linked gene *Cacna1h* in $iKO^{p/q}$ mice reduces thalamic reticular nucleus burst firing and promotes rather than reduces seizure, indicating an epileptogenic role for loss-of-function *Cacna1h* gene variants reported in human childhood absence epilepsy cases. Together, our results demonstrate that P/Q channels remain critical for maintaining normal thalamocortical oscillations and motor control in the adult brain, and suggest that the developmental plasticity of membrane currents regulating pathological rhythmicity is both degenerate and age-dependent.

1 Developmental Neurogenetics Laboratory, Department of Neurology, Baylor College of Medicine, Houston TX, USA
2 Department of Zoology and Neurobiology, Ruhr University of Bochum, Bochum, Germany
3 Department of Neuroscience, Baylor College of Medicine, Houston TX, USA
4 Department of Molecular and Human Genetics, Baylor College of Medicine, Houston TX, USA

Correspondence to: J. L. Noebels
Department of Neurology, Baylor College of Medicine, One Baylor Plaza, Houston TX
77030, USA
E-mail: jnoebels@bcm.edu

Keywords: CACNA1A; childhood absence epilepsy; ataxia; burst firing; CACNA1H

Abbreviations: CAE = childhood absence epilepsy; DP1i = days post-first injection; HCN = hyperpolarization-activated cyclic nucleotide-gated; LD = laterodorsal nucleus; PSD = power spectral density; SWD = spike-and-wave discharge; TRN = thalamic reticular nucleus

Received June 24, 2019. Revised September 9, 2019. Accepted September 29, 2019. Advance Access publication December 4, 2019

Introduction

Synaptic input during early postnatal development is essential to refine adult thalamocortical (Toulmin *et al.*, 2015) and cerebellar function (Kano *et al.*, 2013), and depends upon the fidelity of the release process (Kakizawa *et al.*, 2000) as well as low threshold T-type calcium channel activity (Yoshimura *et al.*, 2008). Disruption of normal synaptic transmission in sensory and motor control pathways during this critical period leads to long-lasting deficits (Kano *et al.*, 2013; Hubener and Bonhoeffer, 2014), but the effects of aberrant transmission initiated after this early period are less understood.

Childhood absence epilepsy (CAE) is a major form of early onset epilepsy that involves abnormal synchronization of thalamocortical networks. It is the most common type of paediatric epilepsy and is clinically diagnosed by a sudden, brief impairment of consciousness, behavioural arrest, and spike-and-wave discharges (SWDs) on EEG (Glauser *et al.*, 2010). The mutant mouse 'tottering' was the first model to reveal a monogenic cause for this disorder (Noebels and Sidman, 1979), which is due to reduced high-voltage activated calcium current ($Ca_v2.1$) through single P/Q-type channels (Fletcher *et al.*, 1996; Wakamori *et al.*, 1998). Loss of function of the orthologous human gene, *CACNA1A*, causes CAE with cognitive deficits and ataxia as well (Rajakulendran *et al.*, 2010; Damaj *et al.*, 2015). Mice with null mutation of *Cacna1a* develop a similar but rapidly progressive neurological deficit including absence epilepsy, ataxia and dystonia and die 3–4 weeks after birth (Jun *et al.*, 1999). However, little is known about whether the distinctive spike-wave seizure and ataxia emerge from developmental defects that would require early therapeutic intervention, or whether they can also arise in a mature network. If the latter is true, it is important to also determine whether mechanisms underlying the spike-wave seizure generation depend upon the same pattern of intrinsic excitability alterations that determine rebound burst firing within the thalamocortical circuit. As absence epilepsy is genetically and physiologically heterogeneous (Maheshwari and Noebels, 2014; Tenney *et al.*, 2014), further insight into the range of pathogenic rebound burst firing properties that sustain spike-wave seizures within this network can provide new insight into human CAE and help develop improved therapies for the disorder.

Here, we examined the consequences of ablating P/Q-type calcium channels in adult mice by tamoxifen-induced genomic recombination. Adult-onset P/Q channel induced knockout mice ($iKO^{p/q}$) showed EEG activity indistinguishable from their control loxP littermates before tamoxifen induction, but rapidly developed the characteristic pattern of ataxia, dystonia, and absence epilepsy within weeks following deletion of P/Q channels upon tamoxifen induction. We found that, in sharp contrast to the inborn models, burst spiking and *Cacna1g*-mediated T-type calcium current (I_T) in thalamocortical relay neurons were not altered in $iKO^{p/q}$ mice. Interestingly, similar to inborn models, loss of *Cacna1g* in $iKO^{p/q}$ mice substantially suppressed SWD generation. Moreover, thalamic reticular nucleus (TRN) burst firing in $iKO^{p/q}$ mice was impaired and accompanied by decreased I_T, which is reversed from inborn models. Deletion of the TRN-enriched and human CAE-linked gene *Cacna1h* in $iKO^{p/q}$ mice slightly reduced TRN burst firing and promoted rather than blocked seizures in these mice. Together, these results demonstrate that P/Q-type calcium channels, which share control of calcium-mediated exocytosis with N- and R-type calcium channels at most central synapses, retain an essential role in normal adult thalamocortical network synchrony, and indicate that inherited childhood absence and ataxia syndromes do not necessarily arise from an irreversible structural perturbation of synaptogenesis during early brain development. The alternative thalamic patterns of pathogenic T-type currents, believed to be a major target of clinical antiepileptic therapy for this seizure type, suggest a possible basis for the treatment failure reported in over 50% of children with this disorder (Glauser *et al.*, 2013).

Materials and methods

Animals

All procedures to maintain and study these mice were conducted with approval of the Institutional Animal Care and Use Committee at Baylor College of Medicine. The $Cacna1a^{Citrine(C57BL/6\ 129/SvJae)}$ ($Cacna1a^{flox/flox}$ for brevity) strain was described in Mark *et al.* (2011). These mice are viable, fertile and display normal P/Q channel function (Mark *et al.*, 2011). The CAGGcre-ER^{TM} [B6.Cg-Tg(CAG-cre/Esr1*)5Amc/J; Stock No: 004682] (*CAG-ER-Cre* for brevity) strain was obtained from the Jackson Laboratory. CAGGcre-ER^{TM} mice express a fusion protein consisting of Cre recombinase and a modified ligand-binding domain of the oestrogen receptor (ER) under the control of the ubiquitous promoter CAG (CMV enhancer, chicken β-actin promoter, rabbit β-globin polyA). The fusion protein only moves into the nucleus upon exposure to tamoxifen, which induces deletion of floxed sequences via Cre-mediated recombination. To prevent Cre leakage, male but not female mice carrying the Cre were used as breeders. In $Cacna1a^{flox/flox}$ mice, a floxed green fluorescent protein derivative Citrine is in the first exon of *Cacna1a*, and exon 1 deletion generates a frame shift to disrupt *Cacna1a* expression. To induce Cre expression, adult mice (>6 week) were injected with a single dose of tamoxifen [dissolved in corn oil, 75 mg/kg body weight, intraperitoneally (i.p.)] per day for five consecutive days. Heterozygous Cre and homozygous loxP mice were used in the experimental group, while homozygous loxP littermates were used as controls unless otherwise stated. Rare Cre leakage was observed in *CAG-ER-Cre*; $Cacna1a^{flox/flox}$ mice older than 4 months indicated by mild ataxia without tamoxifen induction. These mice were excluded in the study. *Cacna1g* knockout mice were generated by breeding heterozygous female mice carrying the *Sox2-Cre* gene [B6.Cg-*Edil3*$Tg^{(Sox2\text{-}cre)1Amc}$/J;

Stock No: 008454] to *Cacna1g*-flox mice [B6(129S4)-*Cacna1g*^{tm1Stl}/J; Stock No: 021932] (Anderson *et al.*, 2005). Both mouse lines were obtained from the Jackson Laboratory. In female *Sox2-cre* mice, Cre recombinase is active in the female germline. Offspring arising from a hemizygous transgenic female exhibit Cre recombinase activity, regardless of genotype. This maternal inheritance effect enables a rapid and efficient generation of null offspring with loxP animals (Hayashi *et al.*, 2002). *Cacna1h* knockout (B6;129-*Cacna1*^{h}^{tm1Kcam}/J; Stock No: 013770) mice were obtained from the Jackson Laboratory. *Cacna1g*$^{-/-}$ and *Cacna1h*$^{-/-}$ mice were crossed with *Cacna1A*^{floxflox};CAG-Cre-ER mice to generate *Cacna1A*^{floxflox};CAG-Cre-ER/*Cacna1g*$^{-/-}$ and *Cacna1A*^{floxflox};CAG-Cre-ER/*Cacna1h*$^{-/-}$, respectively. We used the same tamoxifen induction protocol for these mice. Both male and female mice were studied in all experiments. The number of animals used in each experiment is stated in figure legends.

Polymerase chain reaction

The genetic background of the mice was determined by PCR of genomic DNA from tail or ear biopsy. The following primer pairs were used: (i) *Cacna1a*^{Citrine} forward 5′-TATATCAT GGCCGACAAGCA-3′, reverse 5′-TTCGGTCTTCACAAGG AACC-3′; wild-type (WT) 5′-forward GGGGTCTGACTTCT GATGGA-3′, reverse 5′-AAGTTGCACACAGGGCTTCT-3′; (ii) *Cre* recombinase forward 5′-GCGGTCTGGCAGTA AAAACTATC-3′, 5′-GTGAAACAGCATTGCTGTCACTT-3′; (iii) *Cacna1g*^{tm1Stl} forward 5′-TTCTGCAGCTCTTTCAAT GC-3′, reverse 5′-TGTTCCTACCCAAGGTCTGG-3′; and (iv) *Cacna1h*^{tm1Kcam} mutant forward 5′-GCTAAAGCGCAT GCTCCAGACTG-3′, wild-type forward 5′-ATTCAAGGGCT TCCACAGGGTA-3′, common reverse 5′-CATCTCAGGGCC TCTGGACCAC-3′.

EEG recordings

Mice were anaesthetized with isoflurane (1.5–3% in oxygen, Matrox Vip300 ventilator), and silver wire electrodes (0.005″ diameter) soldered to a connector were surgically implanted bilaterally into the subdural space over frontal and parietal cortex. Mice were allowed to recover for at least 7 days before recording. Simultaneous video-EEG and behavioural monitoring (Labchart 8.0, ADI Systems) was performed in adult (>6 weeks) mice of either sex. EEG was recorded for 4 h while mice moved freely in the test cage on serial days post-first injection (DP1i) (DP1i7, DP1i14, DP1i21 and DP1i28–29) unless otherwise noted. To quantify epileptic activity, the number and duration of SWDs (>0.5-s duration) were visually analysed during the first 30 min of EEG recorded in each mouse. A single dose of ethosuximide (200 mg/kg, i.p.) was injected into iKO$^{p/q}$ mice at DP1i28–29 to test for blockade by this drug. All EEG signals were amplified by a g®.BSAMP biosignal amplifier (Austria), digitized by PowerLab with a 0.5 Hz high-pass and 50 Hz low-pass filter (ADInstruments) and acquired via Labchart 8.0 (ADInstruments). SWDs were identified manually with amplitude larger than twice the root mean square of baseline EEG signal. Power spectral density (PSD) analyses were performed in the Labchart with a FFT (fast Fourier transform) size of 128k (unless otherwise noted) and Hann (cosine-bell) window 50% overlapped.

Rotarod test

After habituation (30 min) in the test room, motor coordination was measured using an accelerating rotarod apparatus (TSE Systems). Mice were tested daily four times (before tamoxifen injection, and at DP1i2, DP1i4 and DP1i7), three trials each, with a rest interval of 60 min between trials. Each trial lasted for a maximum of 10 min, and the rod accelerated from 4 to 40 rpm in the first 5 min. The time that it took for each mouse to fall from the rod (latency to fall) was recorded.

Brain slice preparation

Acute sagittal slices were prepared as previously described (Miao *et al.*, 2016). In brief, the brain was dissected from mice under tribromoethanol (Avertin^{TM}) anaesthesia (250 mg/kg body weight, i.p.), and placed in ice-cold artificial CSF containing (in mM) 125 NaCl, 3 KCl, 2 $CaCl_2$, 2 $MgSO_4$, 1.25 NaH_2PO_4, 1.3 Na^+-ascorbate, 0.6 Na^+-pyruvate, 26 $NaHCO_3$, and 11 glucose (pH 7.4). Sagittal slices (300-µm thick) were cut with a vibratome (VT-1200S, Leica) and incubated in oxygenated protective recovery NMDG (*N*-methyl-D-glucamine) artificial CSF at 34°C for 10–15 min, and then transferred to normal artificial CSF at room temperature (20–25°C) for >45 min before recordings. NMDG artificial CSF contained (in mM) 110 NMDG-Cl, 3 KCl, 0.5 $CaCl_2$, 6 $MgSO_4$, 1.25 NaH_2PO_4, 1.3 Na^+-ascorbate 3, 0.6 Na^+-pyruvate, 26 $NaHCO_3$, and 11 D-glucose (pH 7.4). All recordings were performed in artificial CSF at 32 ± 1°C. Artificial CSF and NMDG artificial CSF were bubbled with 95% O_2/5% CO_2.

Whole-cell recordings

Whole-cell recordings of neurons in the TRN, laterodorsal nucleus (LD), and ventroposterior medial nucleus (VPM) were made with a MultiClamp 700B amplifier (Molecular Devices) as previously described (Miao *et al.*, 2016). LD, VPM and TRN were identified by reference to the Allen Mouse Brain Atlas through an Olympus microscope (5× and 40× objectives, BX-51WIF, Olympus) equipped with infrared video camera and differential interference contrast optics. Signals were filtered at 3 kHz using a Bessel filter and digitized at 10–20 kHz using Digidata 1332A (Molecular Devices). Liquid junction potential was not corrected.

Low-voltage activated transient calcium current (I_T)

I_T was recorded in the presence of tetrodotoxin (TTX, 1 µM, Tocris). A Cs-based internal solution containing (in mM) 125 Cs-gluconate, 5 TEA-Cl, 2 CsCl, 1 EGTA, 10 HEPES, 4 Mg_2ATP, 0.3 Na_2GTP, 10 phosphocreatine (pH 7.2–7.4, 270–310 mOsm) was used (Sun *et al.*, 2010). T current in TRN neurons was recorded in the presence of 10 mM TEA-Cl and 0.5 mM 4-AP in artificial CSF to make cells more electrically compact since TRN neurons have long dendritic processes where T-type calcium channels reside (Joksovic *et al.*, 2005). The perfusion solution contained (in mM) 118 NaCl, 3 KCl, 2 $CaCl_2$, 2 $MgSO_4$, 1.25 NaH_2PO_4, 1.3 Na^+-ascorbate, 0.6 Na^+-pyruvate, 26 $NaHCO_3$, 10 TEA-Cl and 0.5 4-AP and 11 glucose (pH 7.4).

Rebound spiking and membrane excitability

To assess rebound bursting/spiking and firing-input relationships (F-I curve) in thalamocortical neurons, pipettes were filled with an internal solution containing (in mM) 130 K-gluconate, 20 KCl, 10 HEPES, 0.2 EGTA, 4 Mg_2ATP, 0.3 Na_2GTP, and 10 Na_2-phosphocreatine (pH 7.3, 290–310 mOsm). For TRN neurons, the internal solution contained (in mM) 120 K-gluconate, 11 KCl, 1 $MgCl_2$, 1 $CaCl_2$, 10 HEPES, and 1 EGTA, (pH 7.4, 270–290 mOsm) (Clemente-Perez *et al.*, 2017).

Spontaneous inhibitory and excitatory postsynaptic currents

A high chloride internal solution containing (in mM) 94 K-gluconate, 60 KCl, 10 HEPES, 0.2 EGTA, 4 Mg_2ATP, 0.3 Na_2GTP, and 10 Na_2-phosphocreatine (pH 7.3, 290–310 mOsm) was used. To record spontaneous excitatory postsynaptic currents (sEPSCs), neurons were voltage-clamped at –70 mV, with a pipette (resistance of 3–4 MΩ) in the presence of picrotoxin (100 μM) to block GABAergic transmission. To record spontaneous inhibitory postsynaptic currents (sIPSCs), neurons were held at –70 mV in the presence of DNQX (20 μM) and D-AP5 (50 μM) to block AMPARs and NMDARs respectively. Recordings had a typical access resistance of <20 MΩ, and those changed $>30\%$ during recordings were excluded from analyses. Access resistance did not significantly differ between experimental and control groups. sEPSCs and sIPSCs were analysed with MiniAnalysis software (Synaptosoft, Fort Lee, NJ) with a detection threshold of 10 pA followed by manual examination.

Immunohistochemistry and image analysis

Anaesthetized mice [tribromoethanol (Avertin™), 250 mg/kg body weight, i.p.] were perfused with phosphate-buffered saline (PBS, pH 7.4), followed by 4% paraformaldehyde (PFA, w/v) in PBS. Brains were removed and post-fixed in 4% PFA at 4°C for 2 h, then cryoprotected in 30% sucrose (w/v) in PBS for at least 1 day at 4°C. Coronal or sagittal sections (40 μm) were cut on a freezing microtome (Leica) from the fixed brain embedded in optimal cutting temperature (OCT) medium. Slides were thawed at room temperature for 1 h, washed in PBS three times, blocked in a solution containing 10% bovine serum albumin and 0.3% Triton™ X-100 in PBS for 1 h and then overnight with the primary antibody in blocking solution. Slides were washed in blocking solution three times, incubated with the secondary antibody for 2 h, then washed once in blocking solution and three times in PBS before mounting with Antifade mounting medium with DAPI (VECTASHIELD®, Vector Laboratories). The primary antibodies were: rabbit anti-GFP (1:500, Abcam, Cat# ab6556), rabbit anti-Calcium Channel $Ca_v2.1$ (α_{1A} subunit) (1:100, Sigma, Cat# C1353), rabbit anti-Calcium Channel $Ca_v3.1$ (α_{1G} Subunit) (1:300, Alomone, Cat# ACC-021), mouse anti-Tyrosine Hydroxylase (TH, 1:500, Millipore MAB318), anti-Parvalbumin (1:1000, Millipore MAB1572). The secondary antibodies were: Goat anti-Mouse Alexa Fluor® 594 (1:1000 except for 1:500 for TH staining, Thermo Fisher Scientific, Cat# A-21125), Goat anti-Rabbit Alexa Fluor® 488 (1:1000, Thermo Fisher Scientific, Cat# A-11034). Images were acquired on a Nikon C2 laser-scanning confocal microscope with a Plan Apo 20× DIC M (NA = 0.75) or Plan Fluor 10× Ph1 DL objective (NA = 1.4), at 1024 × 1024 pixels. We immunostained GFP to examine the expression of P/Q channels since the α1A subunit is tagged with Citrine (a GFP variant) in the *Cacna1a* floxed mice (Mark *et al.*, 2011). Similar CACNA1A loss in $iKO^{p/q}$ mice was observed with a specific anti-Calcium Channel $Ca_v2.1$ (α_{1A} subunit) antibody (Sigma, Cat# C1353) (data not shown). Immunofluorescence images were captured using the same settings for laser power and detector gain for the same brain region in experimental and corresponding control littermate groups.

Statistics

Data are presented as mean ± standard error of the mean (SEM) with *n* indicating the number of neurons for whole-cell patch-clamp recordings, and the number of animals for immunohistochemistry and EEG datasets. No statistics were used to predetermine sample size. Statistical methods are indicated when used. All analyses were performed using Labchart (8.0), MATLAB (MathWorks), NIS Elements (4.0) and Origin. No method of randomization was used in any of the experiments. Experimenters were not blind to group allocation in behavioural experiments. All animals that finished the entire behavioural testing were included in analysis. All statistical tests were two-sided. For both paired and unpaired tests, we ensured that the variances of the data were similar between the compared groups. For Student *t*-tests, we verified that the data were normally distributed using Jarque-Bera test for normality.

Data availability

Data supporting the findings of this study are available within the article and its Supplementary material. All supporting data in this study are available from the corresponding author on request.

Results

Adult ablation of *Cacna1a* leads to absence seizures and ataxia in mice

To assess the impact of P/Q channel dysfunction beginning in adulthood, we created conditional mice by crossing $Cacna1a^{flox/flox}$ mice with tamoxifen inducible cre line CAGGcre-ER™ (*CAG-Cre-ER* here after) mice (Fig. 1A) . The resulting $Cacna1a^{flox/flox}$;*CAG-Cre-ER* offspring are viable, fertile, and indistinguishable from their $Cacna1a^{flox/flox}$ littermates (Supplementary Video 1). *Cacna1a* is expressed normally in these mice until tamoxifen injection, when a metabolite binds to ER, activating Cre and deleting the first exon. We injected tamoxifen [75 mg/kg, i.p. (intraperitoneal injection)] in $Cacna1a^{flox/flox}$;*CAG-Cre-ER* ($iKO^{p/q}$) mice and their control $Cacna1a^{flox/flox}$ (loxP) littermates at 6–10 weeks of age and probed CACNA1A expression 3 weeks later (Fig. 1B). At this

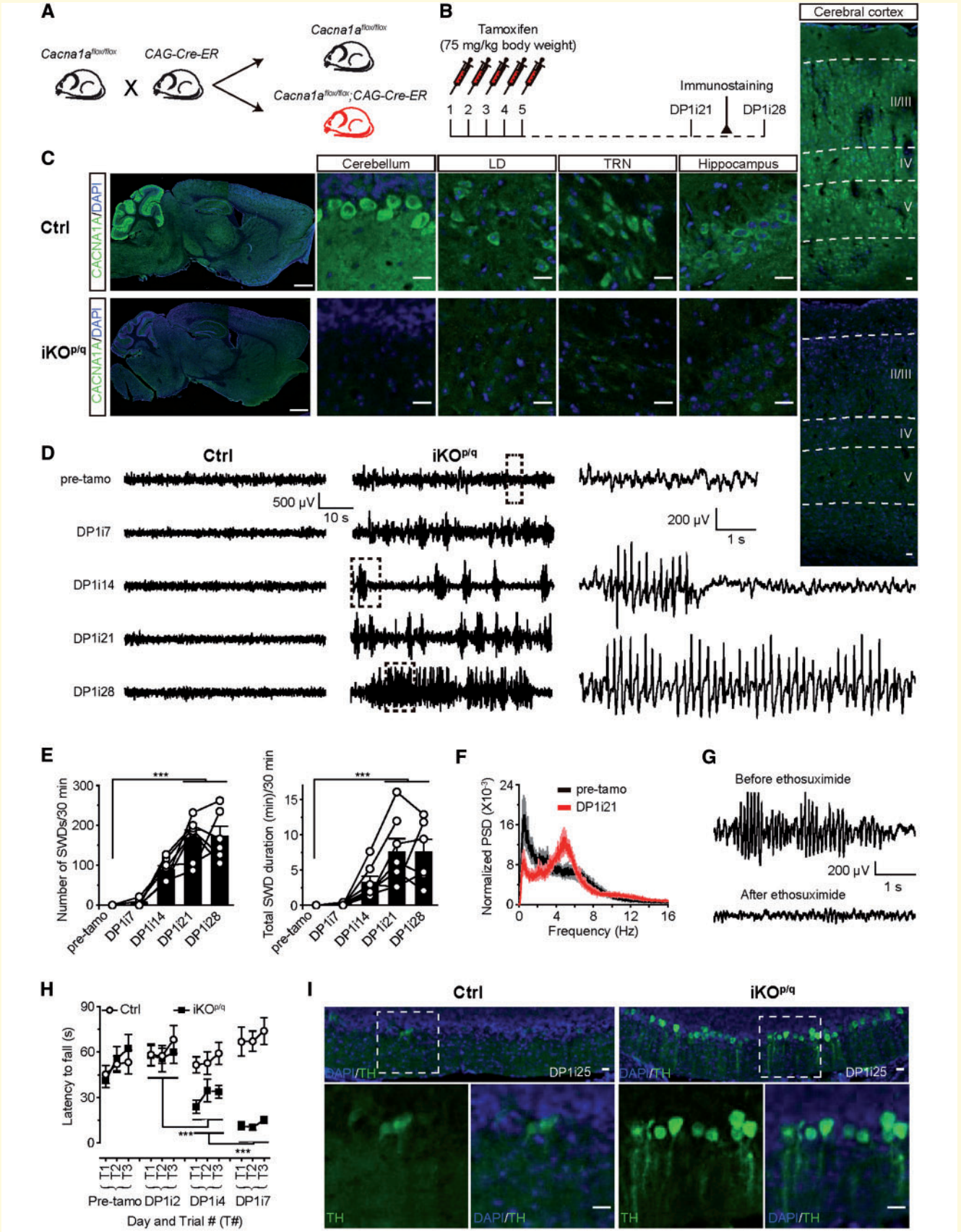

Figure 1 Adult *Cacna1a*$^{flox/flox}$;*CAG-ER-Cre* mice lose CACNA1A after tamoxifen induction and develop spike-wave seizure and ataxia. (**A**) Breeding diagram of *Cacna1a*$^{flox/flox}$;*CAG-ER-Cre* mice and control loxP (*Cacna1a*$^{flox/flox}$) littermates. (**B**) Experimental timeline for (**C**). DP1i21, 28, 21 and 28. (**C**) *Left*: Confocal images showing loss of CACNA1A in an *Cacna1a*$^{flox/flox}$;*CAG-ER-Cre* mouse (iKO$^{p/q}$) compared with

(continued)

time point, CACNA1A protein was greatly reduced throughout the iKO$^{p/q}$ brain, including neocortex, hippocampus, thalamus, and cerebellum compared to control (Fig. 1C) and uninjected *Cacna1a*$^{flox/flox}$;*CAG-Cre-ER* mice (Supplementary Fig. 1). We then assessed how adult loss of the *Cacna1a* gene alters brain rhythms by comparing video-EEG recordings in freely moving animals before, and at DP1i7, DP1i14, DP1i21 and DP1i28. iKO$^{p/q}$ mice showed EEG activity indistinguishable from their control loxP littermates before tamoxifen induction, but progressively developed SWDs with concomitant behavioural arrest within 2 weeks following tamoxifen induction (Fig. 1D, E and Supplementary Video 2) and at later stages (Supplementary Video 3). To exclude potential bias in the manual detection of SWDs, we performed PSD analysis on recorded EEG signals. The appearance of SWD dominant peak frequency (4–6 Hz) was revealed in iKO$^{p/q}$ mice after tamoxifen induction (Fig. 1F and Supplementary Fig. 2A), but not in vehicle-treated *Cacna1a*$^{flox/flox}$;*CAG-Cre-ER* mice (Supplementary Fig. 2B) or tamoxifen induced *Cacna1a*$^{flox/flox}$ (Supplementary Fig. 2C) or *CAG-Cre-ER* mice (Supplementary Fig. 2D). Similar absence seizures were induced in iKO$^{p/q}$ mice older than 4 months and 9 months, respectively (Supplementary Fig. 3). These seizures reproduced those described in spontaneous *Cacna1a* mutants (Noebels and Sidman, 1979). As in inborn P/Q channel genomic mutants, SWDs in all iKO$^{p/q}$ mice (n = 6) were rapidly abolished by systemic injection of ethosuximide, a first choice anti-absence drug (Glauser *et al.*, 2013) (Fig. 1G). Along with absence seizures, iKO$^{p/q}$ mice also developed severe ataxia (Supplementary Video 4). To quantitatively assess the motor deficit, we evaluated their coordination performance on an accelerating rotarod and found a rapidly progressive decline in latency to fall (iKO$^{p/q}$, n = 13; Control, n = 17) (Fig. 1H). We also observed dystonia characteristic of the inborn genomic mutant, accompanied by a similar abnormality in cerebellar cortex of elevated ectopic expression of tyrosine hydroxylase (TH), a distinctive biomarker of Purkinje cell dysfunction (Hess and Wilson, 1991) (Fig. 1I). Together, these results demonstrate that adult loss of P/Q-type calcium channels fully recapitulates the major forebrain and cerebellar inborn neurological phenotypes.

Unaltered burst firing in thalamocortical relay neurons

Burst firing in thalamocortical relay neurons has been widely considered to be essential for thalamocortical rhythmogenesis and SWDs (Huntsman *et al.*, 1999; Kim *et al.*, 2001; McCormick and Contreras, 2001, but see McCafferty *et al.*, 2018). Thalamocortical relay neurons show augmented burst firing and/or low-threshold T-type calcium current (I_T) in various models (Zhang *et al.*, 2002, 2004; Song *et al.*, 2004; Cheong *et al.*, 2009; Ernst *et al.*, 2009; Bomben *et al.*, 2016). We first examined rebound burst responses to membrane hyperpolarization in thalamocortical relay neurons in brain slices from iKO$^{p/q}$ mice and control loxP littermates. LD and VPM thalamic nuclei, were selected because LD projects to frontal cortical regions in which cortical SWDs in inborn mutants predominate (Zhang *et al.*, 2002), and SWDs are thought to be initiated in the somatosensory cortex targeted by VPM (Meeren *et al.*, 2002; Polack *et al.*, 2007). In all neurons tested, a hyperpolarization was followed by rebound excitation characterized by a burst of action potentials riding on a low-threshold calcium depolarization/spike (LTS). However, there was no significant difference in the number of burst spikes or the peak amplitude of the LTS compared to control mice in either the LD (Fig. 2A–C and Supplementary Fig. 4A and B) or VPM (Supplementary Fig. 4E). No differences were detected in the injected current, membrane capacitance or resistance (Fig. 4D and E). We then directly measured I_T via whole-cell voltage-clamp recordings and found that this current was unaffected (Fig. 2I and J). These results demonstrate that burst firing mediated by I_T in thalamocortical relay neurons remains unchanged following adult P/Q channel excision. No change in the tonic firing of LD neurons was found in iKO$^{p/q}$ mice either (Supplementary Fig. 4C and D). Interestingly, we found a reduced depolarizing sag in iKO$^{p/q}$ thalamocortical realy neurons (Fig. 2F, G and Supplementary Fig. 4F), indicating downregulation of hyperpolarization-activated current (I_h) mediated by hyperpolarization-activated cyclic nucleotide-gated (HCN) channels. Consistent with this finding, the resting membrane potential in these cells was significantly shifted toward more hyperpolarized value by 3.1 mV on average (Fig. 2H).

Figure 1 Continued

control littermate (Ctrl) after tamoxifen induction (DP1i25). Scale bars = 1 mm. *Right*: Magnified images show the loss in the cerebellum cortex, thalamic LD and TRN, hippocampus, and cerebral cortex. Nuclei were labelled with 4′,6-diamidino-2-phenylindole (DAPI). Scale bars = 20 μm. (**D**) Representative EEG traces from control and iKO$^{p/q}$ mice before (pre-tamo) and after tamoxifen induction. *Right*: Expanded traces show the three boxed areas. Note the development of spontaneous SWDs in iKO$^{p/q}$ mice. (**E**) Summary graphs for the total number (*left*) and total duration (*right*) of SWDs in 30 min for iKO$^{p/q}$ mice. Kolmogorov–Smirnov test, $^{***}P < 0.001$. (**F**) PSD (solid line, averaged; shadow, SEM) shows the dominant frequency (4–6 Hz) of SWDs in iKO$^{p/q}$ mice (n = 7) at DP1i21 compared with that before tamoxifen induction. PSD was normalized to total PSD under 50 Hz. (**G**) Representative EEG traces show that ethosuximide (200 mg/kg body weight, i.p.) abolished SWDs from iKO$^{p/q}$ mice (n = 6). (**H**) iKO$^{p/q}$ mice (n = 13), but not control (n = 17) show a progressively shorter latency to fall on a rotarod after tamoxifen induction. Two-way (genotype × trial) ANOVA with repeated measures, $^{***}P < 0.001$. (**I**) Confocal images show enhanced expression of TH in the vermis of cerebellum from iKO$^{p/q}$ mice compared with control. Scale bars = 20 μm. Mean ± SEM.

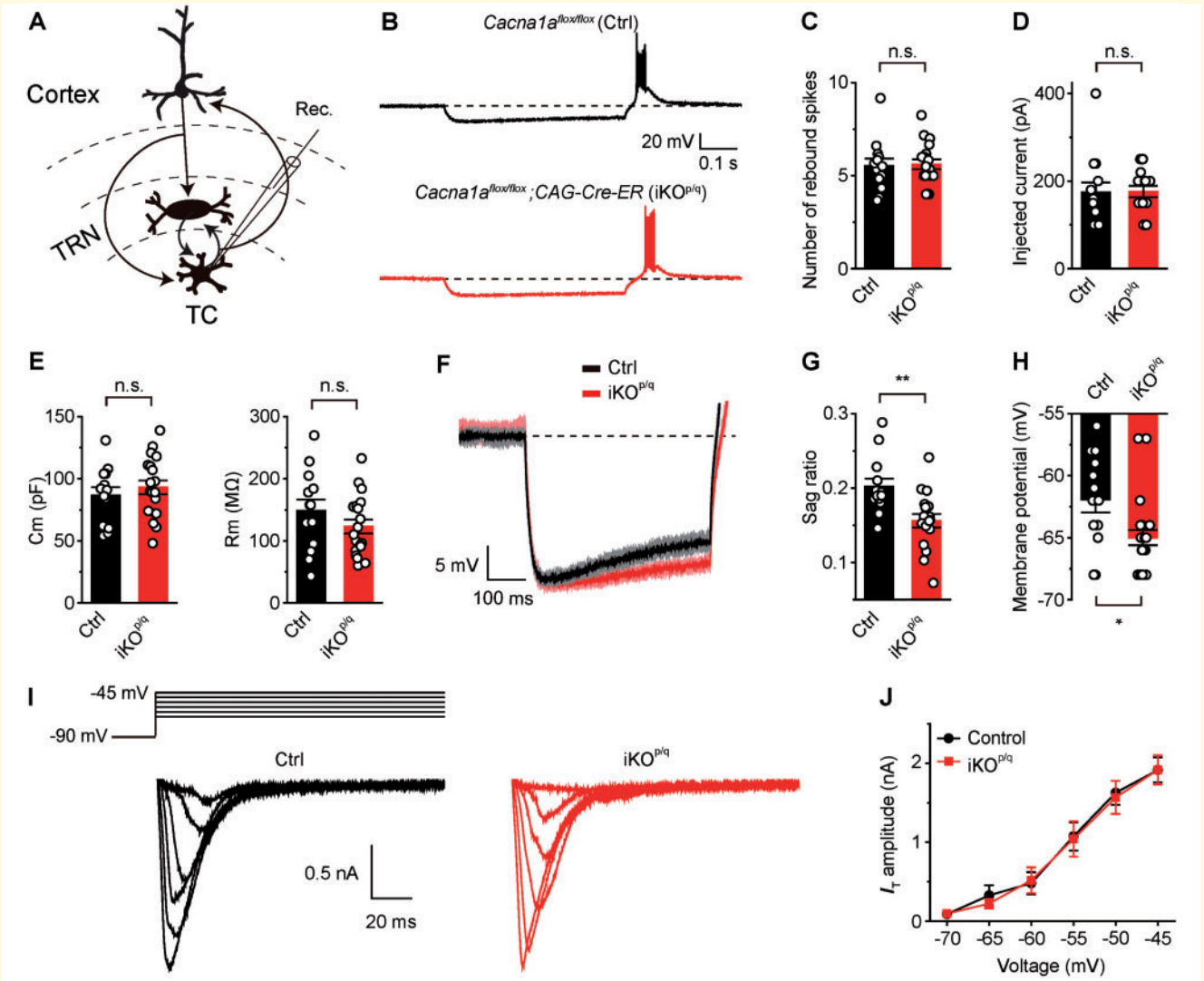

Figure 2 Adult *Cacna1a* loss reduces voltage sag and hyperpolarizes resting membrane potential in thalamic laterodorsal neurons. (**A**) Schematic of whole-cell recording experiments. Rec. = recording electrode. (**B**) Representative rebound spiking of thalamocortical neurons from tamoxifen-induced control loxP and iKO$^{p/q}$ mice in response to a hyperpolarizing current step. (**C**) Summary graph for the number of rebound spikes in the thalamic LD neurons of control and iKO$^{p/q}$ mice. On average, the number of rebound spikes is similar (control: n = 13; iKO$^{p/q}$: n = 18). Kolmogorov–Smirnov test, P = 0.99. (**D** and **E**) current injected, membrane capacitance (Cm) and resistance (Rm) are similar. (**F**) Representative responses (solid line, averaged; shadow, repeats) to a hyperpolarizing current step into LD neurons (160 and 100 pA, respectively). (**G** and **H**) Summary graphs for sag ratio (**G**) and resting membrane potential (**H**). Depolarizing sag is smaller and the average resting membrane potential is more hyperpolarized in LD neurons from iKO$^{p/q}$ mice compared with control. Student's t-test. (**I**) T-type calcium current (I_T) recorded from LD neurons in response to test potentials ranging from –70 to –45 mV after being hyperpolarized (2–3 s) to –90 mV. Traces are aligned to the mean of the last 50 ms. (**J**) Summary graph of the peak amplitude of I_T (control: n = 10; iKO$^{p/q}$: n = 10). The average amplitude of I_T in iKO$^{p/q}$ mice is similar to that in control mice. Student's t-test. P = 0.99. $^*P < 0.05$, $^{**}P < 0.01$. n.s. = not significant. Mean ± SEM. TC = thalamocortical relay neuron.

Loss of burst spiking in the thalamocortical relay neurons diminishes seizure generation

Burst firing in thalamocortical relay neurons is mediated by low threshold-activated T-type Ca^{2+} channels $Ca_v3.1$ (Kim *et al.*, 2001). Its pore-forming α subunit is encoded by *Cacna1g*. To determine directly whether the generation of spontaneous SWDs in our adult-onset model depends on burst firing in thalamocortical neurons, we eliminated *Cacna1g*-mediated currents in iKO$^{p/q}$ mice by generating *Cacna1a*$^{flox/flox}$;*CAG-Cre-ER*;*Cacna1g*$^{-/-}$ mice (iKO$^{p/q+g}$). Deletion of α1G was confirmed by immunohistochemistry using its specific antibody (Supplementary Fig. 5). In iKO$^{p/q+g}$ mice, I_T and burst firing were abolished in thalamocortical relay neurons (Fig. 3A–C). Interestingly, a similar decrease in the sag response of LD neurons (sag ratio: 0.157 ± 0.019; Student's t-test; P = 0.032) was found in

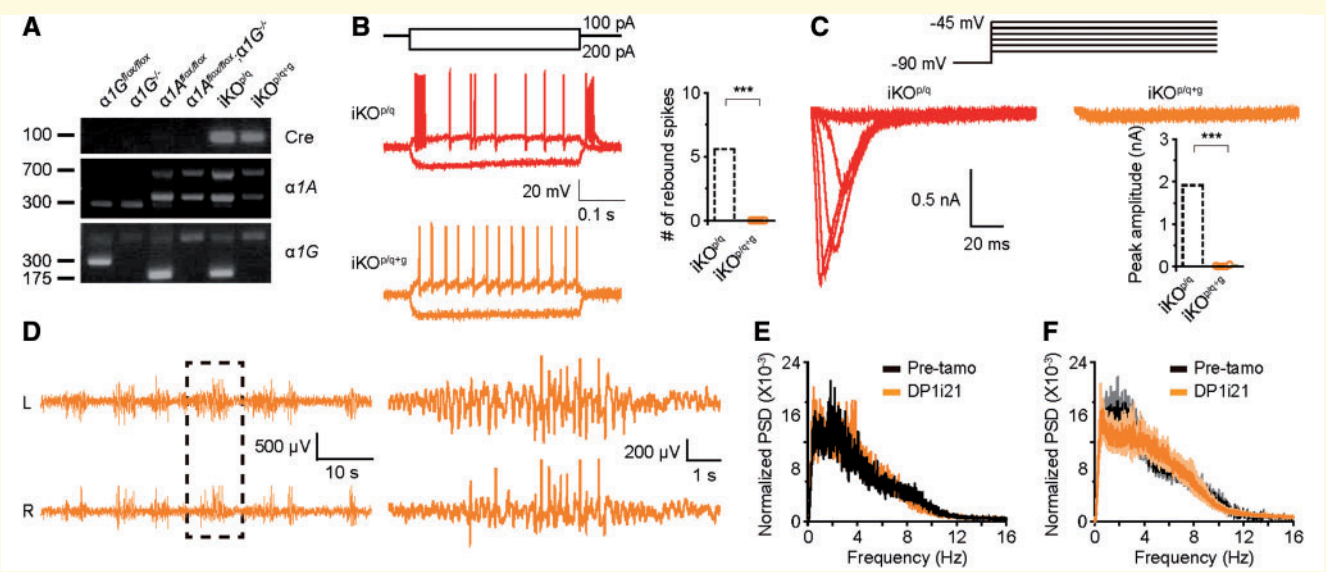

Figure 3 α1G deficiency suppresses but does not prevent absence seizure in *Cacna1a* adult-ablated mice. (**A**) PCR results for genotyping *Cacna1a* $^{flox/flox}$;*CAG-ER-Cre*;*Cacna1G*$^{-/-}$ (iKO$^{p/q+g}$) mice. The *Cre* primers generated a 100-bp product. The *Cacna1a* primers generated a 300-bp band for the wild-type or two bands (400 bp and 700 bp) for the loxP-flanked allele. The *Cacna1g* primers produced a 175-bp band for the wild-type, a 300-bp product for the floxed allele or a 700-bp product for knockout allele. (**B**) Representative responses to a hyperpolarizing current (200 pA) and a depolarizing current (100 pA) in LD neurons from iKO$^{p/q}$ and iKO$^{p/q+g}$ mice. No rebound spike was evoked in LD neurons (n = 9) from iKO$^{p/q+g}$ mice as shown in bar graph. Student's t-test. $^{***}P < 0.001$. (**C**) Representative T-type calcium current (I_T) recorded from LD neurons in response to test potentials from –90 mV in tamoxifen induced iKO$^{p/q}$ (DP1i23) and iKO$^{p/q+g}$ (DP1i31) mice. *Bottom right*: Summary graph of the peak amplitude of I_T (iKO$^{p/q+g}$: n = 5). On average, the amplitude of I_T in iKO$^{p/q+g}$ mice is 9.91 ± 7.51 pA. Student's t-test. $^{*}P <$ 0.001. (**D**) Representative EEG traces (two channels, L and R) show spontaneous spike-wave-discharges (SWDs) from a tamoxifen induced iKO$^{p/q+g}$ mouse (DP1i21). Expanded traces show the boxed area. (**E**) PSD analysis shows that unlike iKO$^{p/q}$ mice, a similar PSD distribution in the iKO$^{p/q+g}$ mouse at DP1i21 to that before tamoxifen induction (Pre-tamo). (**F**) Summary graph for PSD before and after tamoxifen induction for iKO$^{p/q+g}$ mice. Mean ± SEM.

tamoxifen induced iKO$^{p/q+g}$ mice compared with control *Cacna1a* loxP mice. We recorded vEEG in adult iKO$^{p/q+g}$ mice (n = 6) before (averaged age: 52.2 ± 1.1 days) and after tamoxifen induction, and found that after tamoxifen injection, all iKO$^{p/q+g}$ mice displayed similar SWDs to those observed in iKO$^{p/q}$ mice (Fig. 3D–F), although with a greatly reduced occurrence (DP1i21, SWDs number and total duration in 30 min: 37.7 ± 25.4; 102.5 ± 74.8 s, Kolmogorov–Smirnov test, P = 0.0087 compared with iKO$^{p/q}$ mice at DP1i21, 169.1 ± 20.0; 454.0 ± 113.8 s; Fig. 1E). iKO$^{p/q+g}$ mice also developed severe ataxia after tamoxifen induction as iKO$^{p/q}$ mice (data not shown). In addition, *Cacna1g* knockout mice (*Cacna1g*$^{-/-}$) did not exhibit spontaneous SWD before or after tamoxifen induction (data not shown). These results demonstrate that *Cacna1g* is not strictly necessary for the adult generation of absence seizure, but still remains critical for the generation of SWDs as in inborn models.

Impaired burst firing in the thalamic reticular nucleus

Thalamocortical relay neurons and TRN neurons form a reciprocal excitatory-inhibitory network. Enhanced burst firing in the TRN is widely believed to be essential for the generation of abnormal thalamocortical oscillations underlying absence epilepsy in multiple genetic models (Tsakiridou *et al.*, 1995; Broicher *et al.*, 2008; McCafferty *et al.*, 2018). To examine the burst firing of TRN neurons, we performed *in vitro* whole-cell recordings. Unexpectedly, we found a significant impairment of burst firing (Fig. 4A–E and Supplementary Fig. 6A–C) along with reduced membrane excitability (Rheobase: Control, 47.6 ± 7.6 pA; iKO$^{p/q}$, 57.3 ± 7.7 pA; Kolmogorov–Smirnov test. P = 0.66; Fig. 4F and G) in these cells in iKO$^{p/q}$ mice compared with control loxP littermates. TRN neuron resting membrane potential was increased in iKO$^{p/q}$ mice (Supplementary Fig. 6D). A consistent decrease in I_T was found in TRN neurons (Fig. 4H and G). Interestingly, in tamoxifen induced iKO$^{p/q+g}$ mice, a similar decrease in the burst spiking of TRN neurons was found (1.33 ± 0.76 rebound spikes; n = 14; Mann–Whitney U-test P = 0.0056 compared with control *Cacna1a* loxP mice, 8.27 ± 2.30 rebound spikes; n = 22). We also found an increase in the frequency of sIPSCs, rather than sEPSCs onto TRN neurons in iKO$^{p/q}$ mice (Supplementary Fig. 7A and B), This finding implicates increased inhibition from GABAergic neurons located in other brain regions that target TRN [as adult mice lack intra-TRN GABAergic connections (Hou *et al.*, 2016)], or possibly new formation of

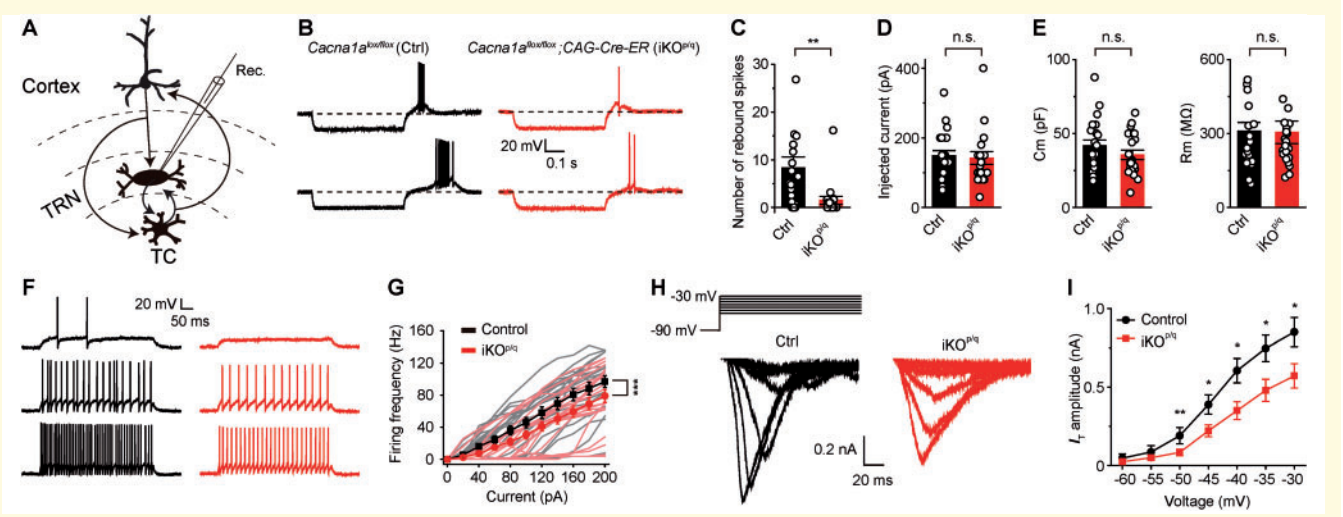

Figure 4 Adult *Cacna1a* ablation results in reduced rebound spiking and membrane excitability of neurons in TRN. (**A**) Schematic of whole-cell recording experiments. (**B**) Representative rebound spiking of TRN neurons from tamoxifen induced control loxP and iKO$^{p/q}$ mice in response to a hyperpolarizing current step. (**C**) Summary graph of the number of rebound spikes (control: n = 22; iKO$^{p/q}$: n = 23). The average number of TRN rebound spikes in iKO$^{p/q}$ mice is smaller than that for control mice. Mann–Whitney U-test. $^{**}P < 0.01$. (**D** and **E**) Current injected, membrane capacitance and resistance are similar. (**F**) As in **B**, but for tonic firing in response to a series of depolarizing current steps. (**G**) Summary graph shows firing frequency versus the amplitude of injected current (individual neuron: grey and light red lines; average: black filled square and red filled circle) for TRN neurons (control: n = 21; iKO$^{p/q}$: n = 22). N-way ANOVA. $^{***}P < 0.001$. (**H**) T-type calcium current (I_T) recorded from TRN neurons in response to test potentials ranging from –60 to –30 mV after being hyperpolarized (2–3 s) to –90 mV. Traces are aligned to the mean of the last 50 ms. (**I**) Summary graph of the peak amplitude of I_T (control: n = 18; iKO$^{p/q}$: n = 17). On average, the amplitude of I_T in iKO$^{p/q}$ mice is smaller compared with control. Student's t-test. $^{*}P < 0.05$. Mean ± SEM. TC = thalamocortical relay neuron.

intra-TRN GABAergic synapses induced by P/Q channel ablation. In contrast, the frequency and amplitude of sIPSCs and sEPSCs onto thalamic relay neurons remained unchanged (Supplementary Fig. 7C and D). Together, these results demonstrate that burst firing in TRN is impaired in mice with adult-onset P/Q channel ablation and suggest that suppressing, rather than promoting TRN excitability might be essential for generating adult-onset absence seizures.

Loss of *Cacna1h* promotes seizure generation

Burst firing in TRN is mediated by two subtypes of T-type calcium channels, $Ca_v3.2$ and $Ca_v3.3$ (encoded by *Cacna1h* and *Cacna1i*, respectively) (Talley *et al.*, 1999). The $Ca_v3.2$-encoding gene *CACNA1H* has been associated with human CAE in genetic studies (Chen *et al.*, 2003*b*; Heron *et al.*, 2007). The significance of *CACNA1H* in CAE is further heightened by the fact that nearly half of patients with CAE failed in treatment with ethosuximide, a front line anti-CAE drug (Coulter *et al.*, 1989; Glauser *et al.*, 2010; Wang *et al.*, 2015). How *CACNA1H* mutations contribute to CAE is, however, unclear. In addition, unlike $Ca_v3.1$ and $Ca_v3.3$, the role of $Ca_v3.2$ in SWDs has not been explored by genetic deletion (Lee *et al.*, 2014). To address this question, we generated *Cacna1a*$^{flox/flox}$;*CAG-Cre-ER*;*Cacna1h*$^{-/-}$mice (iKO$^{p/q+h}$) to examine the effect of adult P/Q deletion on a *Cacna1h*$^{-/-}$ background (Chen *et al.*, 2003*a*) (Fig. 5A). The additional knockout of *Cacna1h* slightly reduced burst spiking and membrane excitability in TRN neurons to a level comparable to tamoxifen induced iKO$^{p/q}$ mice (Fig. 5B–D). We recorded EEG activity from these mice before and after tamoxifen induction. Surprisingly, we found that tamoxifen reliably induced SWDs in all iKO$^{p/q+h}$ mice, similar to iKO$^{p/q}$ mice (Fig. 5E and F); indeed, SWD duration, which purportedly depends upon rebound burst firing, was even longer (Fig. 5G). All iKO$^{p/q+h}$ mice also developed severe ataxia after tamoxifen induction as seen in iKO$^{p/q}$ mice (data not shown). Together, these results indicate a potential downstream role of *Cacna1h* reduction in favouring the generation of absence epilepsy due to adult-onset P/Q calcium channel dysfunction. Consistent with our findings, further suppression of rebound burst firing in *Cacna1i*-deficient TRN neurons by *Cacna1h* deletion did not abolish, but instead enhanced pharmacologically-induced absence seizures in adult mice (Lee *et al.*, 2014).

Discussion

We established an adult-onset animal model through tamoxifen induced ablation of P/Q-type calcium channels for childhood absence epilepsy, and determined that the

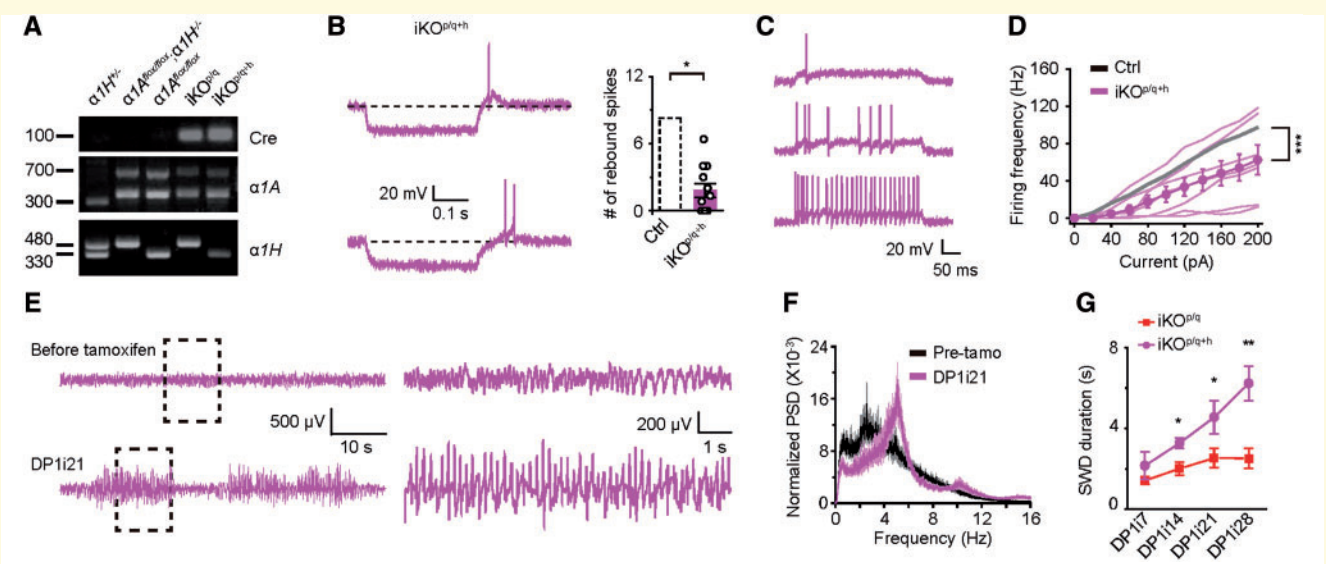

Figure 5 ***Cacna1h*** **null mutation results in reduced TRN excitability and prolonged SWDs in** ***Cacna1a*** **adult-ablated mice.** (**A**) PCR results for genotyping *Cacna1a*$^{flox/flox}$;*CAG-ER-Cre*;*Cacna1h*$^{-/-}$ (iKO$^{p/q+h}$) mice. The *Cre* primers generated a 100-bp product. The *Cacna1a* primers generated a 300-bp band for the wild-type or two bands (400 bp and 700 bp) for the loxP-flanked allele. The *Cacna1h* primers produced a 480-bp band for the wild-type or a 330-bp product for the knockout allele. (**B**) *Left*: Representative responses to a hyperpolarizing step current injected into TRN neurons in iKO$^{p/q+h}$ mice without tamoxifen induction. *Right*: Summary graph shows fewer rebound spikes in TRN neurons from iKO$^{p/q+h}$ mice (n = 12) compared with *Cacna1a*$^{flox/flox}$ mice (Ctrl, dash bar). Mann–Whitney U-test. $^{*}P < 0.05$. (**C**) As in **B**, but for tonic firing in response to a series of depolarizing current steps. (**D**) Summary graph shows firing frequency versus the amplitude of current injected (individual neuron: light magenta lines; averaged: magenta filled circle and grey line) for TRN neurons (iKO$^{p/q+h}$: n = 7). TRN neuron from iKO$^{p/q+h}$ mice is less excitable compared with *Cacna1a*$^{flox/flox}$ mice (Ctrl, grey line). N-way ANOVA. $^{***}P < 0.001$. (**E**) Representative EEG traces show spontaneous SWDs from an iKO$^{p/q+h}$ mouse induced by tamoxifen injection. Expanded traces show the boxed areas. (**F**) PSD analysis shows the dominant frequency (4–6 Hz) of SWDs in iKO$^{p/q+h}$ mice (n = 5) at DP1i21 compared with that before tamoxifen induction (Pre-tamo). (**G**) Bar graph shows that the average duration of SWDs from iKO$^{p/q+h}$ mice is longer compared with iKO$^{p/q}$ mice. Student's t-test. $^{*}P < 0.05$, $^{**}P < 0.01$. Mean ± SEM.

thalamocortical synchronization disorder in the mature brain arises from distinct thalamic circuit dynamics compared with inborn models.

Adult-onset P/Q channel deletion in mice recapitulates childhood absence epilepsy

Previous studies demonstrated that genomic loss of P/Q calcium channels shifts the reliance of excitation-release coupling at central synapses to more loosely coupled N- and R-type channels (Midorikawa *et al.*, 2014), and when limited to a single presynaptic corticothalamic input, trans-synaptically elevates T-type calcium current in postsynaptic thalamic neurons, leading to absence epilepsy (Bomben *et al.*, 2016). Here, through loss-of-function experiments, we demonstrate that P/Q calcium channels remain essential for regulating brain rhythomogenesis and motor functions in the adult animal, and show that a key cerebellar endophenotype (ectopic expression of TH) is also recapitulated in our model. Together, these results demonstrate a development-independent role of P/Q calcium channels in the generation of epilepsy and ataxia due to mutation of *Cacna1a*.

The role of $Ca_v3.1$-mediated burst firing in absence epilepsy

Numerous studies have supported the idea that repetitive burst firing of thalamocortical relay neurons plays a key role in the generation of SWDs, manifest as hyper-synchronized episodic oscillation activities in the thalamocortical network. However, there is now increasing controversy on this point (Huguenard, 2019). Burst firing in the thalamocortical relay neurons is mediated by *Cacna1g* ($Ca_v3.1$ channels). Despite the fact that overexpression of *Cacna1g* promotes SWD (Ernst *et al.*, 2009), we found, as have others (Song *et al.*, 2004), that $Ca_v3.1$ deletion suppressed SWDs in *Cacna1a* mutants to a significant extent, even in the adult-onset model. Our results support the notion that $Ca_v3.1$-mediated thalamocortical burst firing is essential for the generation of SWDs, although it is possible that loss of $Ca_v3.1$ in brain regions other than thalamus, such as neocortex, is responsible for the suppression. Region specific $Ca_v3.1$ channel manipulation is required to test this idea in the future. It is noteworthy that $Ca_v3.1$ null mutation completely abolished SWDs in inborn α1A knockout mice (although these mice died around 3–4 weeks after birth) (Jun *et al.*, 1999; Song *et al.*, 2004), whereas loss of $Ca_v3.1$ does

not completely block SWDs in our adult-onset P/Q channel deleted mice ($iKO^{p/q+g}$), similar to the results found after removing $Ca_v3.1$ in three other mutants with absence seizures, i.e. tottering ($\alpha 1A^{tg/tg}$), lethargic ($\beta 4^{lh/lh}$), or stargazer ($\gamma 2^{stg/stg}$) (Song *et al.*, 2004).

Burst firing in thalamocortical relay neurons is regulated by various ion channels, including HCN channels. Homo- or heterotetrameric channels are formed by four HCN channel subunits (HCN1–4) that display a distinct pattern of distribution in the nervous system (Santoro *et al.*, 2000; Notomi and Shigemoto, 2004). Loss of HCN1 subunits promotes epileptogenesis in mice and HCN1-deficient rat and HCN2-deficient mice exhibit spontaneous absence seizures (Ludwig *et al.*, 2003; Chung *et al.*, 2009; Huang *et al.*, 2009; Nishitani *et al.*, 2019), while pharmacological blockade or local antisense reduction of HCN channels in thalamocortical relay neurons suppress SWDs in two genetic models (Cain *et al.*, 2015; David *et al.*, 2018). Although the number of spikes in a rebound burst evoked by hyperpolarization was not altered in the thalamocortical relay neurons of $iKO^{p/q}$ mice, we found a significant reduction in the depolarizing sag response that is likely mediated by HCN channels. How this change affects thalamocortical relay neuron burst firing *in vivo* and contributes to the generation of SWDs remains to be investigated. Further studies are also warranted to investigate how HCN channels are regulated. It is noteworthy that HCN channels could form a complex with $Ca_v3.2$ channels (Fan *et al.*, 2017), implying that the HCN and $Ca_v3.2$ channels might be co-regulated by the same signalling pathway in $iKO^{p/q}$ mice upon P/Q channel ablation.

Epileptogenic regulation of absence epilepsy by the *CACNA1H* gene

Altered low-threshold bursting in TRN neurons has been hypothesized to drive thalamocortical hyper-synchrony underlying SWDs (Tsakiridou *et al.*, 1995; Cain *et al.*, 2018; McCafferty *et al.*, 2018). In contrast, complete loss of burst firing in TRN neurons does not prevent but rather promote pharmacologically induced SWDs in mice with compound deletion of both $Ca_v3.2$ and $Ca_v3.3$ (Lee *et al.*, 2014). Similar results were found in $Ca_v3.3$ knockout mice in the same study. How loss of $Ca_v3.2$ alone affects SWD generation has not previously been examined in a genetic absence seizure model. Some mutations found in human CAE patients were shown to be gain-of-function in heterologous cells; however, the majority had no effect on the biophysical properties of $Ca_v3.2$ channels (Khosravani *et al.*, 2004, 2005; Peloquin *et al.*, 2006), suggesting that epilepsy-related mutations in *CACNA1H* might affect seizure threshold via regulating channel trafficking or RNA splicing rather than directly mediating biophysical changes in pore dynamics the channels (Khosravani and Zamponi, 2006; Proft *et al.*, 2017). In one study, absence epilepsy was not found in $Ca_v3.2$ knockout mice, although it was reported that $Ca_v3.2$ knockout mice had longer slow-wave (non-rapid-eye-movement) sleep bouts (Pellegrini *et al.*, 2016). Nonetheless, our results support a seizure promoting role for *Cacna1h* gene loss-of-function in a genetic absence seizure model. This ancillary role may bear on the current controversy over the contribution of TRN and thalamocortical neuron bursting underlying SWD generation (Huguenard, 2019).

It has been recently reported that local infusion of a T-type calcium channels blocker, TTA-P2 in ventrobasal thalamus had no effect on absence seizures (McCafferty *et al.*, 2018). One explanation for this result might be that the pharmacological action of this agent on $Ca_v3.1$ and $Ca_v3.2$ obscures the individual contribution of each T-type channel, since TTA-P2 blocks all three T-type calcium channels (Shipe *et al.*, 2008). In addition, other than contributing to bursting properties of TRN neurons, $Ca_v3.2$ is also expressed at axon terminals and regulates synaptic transmission (Huang *et al.*, 2011; Wang *et al.*, 2015), although whether $Ca_v3.2$ is expressed at TRN presynaptic terminals targeting thalamocortical relay neurons and its role in synaptic transmission remains to be determined. A similar confounding effect might explain the ability of ethosuximide to block SWD generation in our model, as intraperitoneal ethosuximide acts throughout the thalamocortical circuit. Without minimizing the contribution of intracortical circuitry to spike-wave seizure generation, our analysis focuses on the role of thalamic rhythm generation.

Circuit heterogeneity and network burst disparity underlying corticothalamic dysrhythmia

Based on prior studies and our results, we propose that excitability changes in thalamocortical circuits generating SWDs are heterogeneous and that some SWDs, at least in mouse genetic models, can be generated by variable sets of conductance distributed within these circuits. In support of this view, circuit heterogeneity is well established in human disorders featuring SWDs (Blumenfeld, 2005; Tenney *et al.*, 2014). Our findings provide direct support for degenerate current profiles underlying pathogenic rhythmic behaviour in the mouse thalamocortical circuitry. Namely, the precisely regulated burst patterns within this tightly-coupled network involving neocortex, TRN, and thalamo-cortical relay neurons, may arise from flexible sets of underlying conductances. This seminal construct, supported by analysis of a tri-cellular circuit in a crustacean ganglion and *in silico* modelling (Gutierrez and Marder, 2014; O'Leary *et al.*, 2014), predicts not only a spectrum of homeostatic membrane excitability properties driving stable oscillatory rhythms at various ages, but also multiple, and perhaps age-dependent therapeutic solutions for restoring normal circuit behaviour. Our evidence demonstrates that P/Q-type calcium channels, which share control of calcium-mediated exocytosis with N- and R-type channels at most

central synapses, retain an essential role in normal adult cortical network synchrony, and indicate that inherited childhood absence and ataxia syndromes do not necessarily arise from an irreversible structural perturbation of synaptogenesis during early brain development. Adult deletion of P/Q channels also provides novel insight into the persistent plasticity of downstream thalamic T-type currents in adult mice, revealing cell and age-specific patterns of homeostatic remodelling that may serve as new targets for reversing neurological disorders mediated by the P/Q-type calcium channel.

Acknowledgements

We thank Drs I. Aiba and N. Josset for their critical comments on this manuscript.

Funding

This work was supported by NINDS NS29709 (J.L.N.).

Competing interests

The authors report no competing interests.

Supplementary material

Supplementary material is available at *Brain* online.

References

Anderson MP, Mochizuki T, Xie J, Fischler W, Manger JP, Talley EM, et al. Thalamic Cav3.1 T-type Ca2 + channel plays a crucial role in stabilizing sleep. Proc Natl Acad Sci U S A 2005; 102: 1743–8.

Blumenfeld H. Cellular and network mechanisms of spike-wave seizures. Epilepsia 2005; 46: 21–33.

Bomben VC, Aiba I, Qian J, Mark MD, Herlitze S, Noebels JL. Isolated P/Q calcium channel deletion in layer VI corticothalamic neurons generates absence epilepsy. J Neurosci 2016; 36: 405–18.

Broicher T, Kanyshkova T, Meuth P, Pape HC, Budde T. Correlation of T-channel coding gene expression, IT, and the low threshold Ca2 + spike in the thalamus of a rat model of absence epilepsy. Mol Cell Neurosci 2008; 39: 384–99.

Cain SM, Tyson JR, Choi HB, Ko R, Lin PJC, LeDue JM, et al. CaV 3.2 drives sustained burst-firing, which is critical for absence seizure propagation in reticular thalamic neurons. Epilepsia 2018; 59: 778–91.

Cain SM, Tyson JR, Jones KL, Snutch TP. Thalamocortical neurons display suppressed burst-firing due to an enhanced Ih current in a genetic model of absence epilepsy. Pflugers Archiv 2015; 467: 1367–82.

Chen CC, Lamping KG, Nuno DW, Barresi R, Prouty SJ, Lavoie JL, et al. Abnormal coronary function in mice deficient in alpha1H T-type Ca2 + channels. Science 2003a; 302: 1416–8.

Chen Y, Lu J, Pan H, Zhang Y, Wu H, Xu K, et al. Association between genetic variation of CACNA1H and childhood absence epilepsy. Ann Neurol 2003b; 54: 239–43.

Cheong E, Zheng Y, Lee K, Lee J, Kim S, Sanati M, et al. Deletion of phospholipase C beta4 in thalamocortical relay nucleus leads to absence seizures. Proc Natl Acad Sci U S A 2009; 106: 21912–7.

Chung WK, Shin M, Jaramillo TC, Leibel RL, LeDuc CA, Fischer SG, et al. Absence epilepsy in apathetic, a spontaneous mutant mouse lacking the h channel subunit, HCN2. Neurobiol Dis 2009; 33: 499–508.

Clemente-Perez A, Makinson SR, Higashikubo B, Brovarney S, Cho FS, Urry A, et al. Distinct thalamic reticular cell types differentially modulate normal and pathological cortical rhythms. Cell Rep 2017; 19: 2130–42.

Coulter DA, Huguenard JR, Prince DA. Characterization of ethosuximide reduction of low-threshold calcium current in thalamic neurons. Ann Neurol 1989; 25: 582–93.

Damaj L, Lupien-Meilleur A, Lortie A, Riou E, Ospina LH, Gagnon L, et al. CACNA1A haploinsufficiency causes cognitive impairment, autism and epileptic encephalopathy with mild cerebellar symptoms. Eur J Hum Genet 2015; 23: 1505–12.

David F, Carcak N, Furdan S, Onat F, Gould T, Meszaros A, et al. Suppression of hyperpolarization-activated cyclic nucleotide-gated channel function in thalamocortical neurons prevents genetically determined and pharmacologically induced absence seizures. J Neurosci 2018; 38: 6615–27.

Ernst WL, Zhang Y, Yoo JW, Ernst SJ, Noebels JL. Genetic enhancement of thalamocortical network activity by elevating alpha 1g-mediated low-voltage-activated calcium current induces pure absence epilepsy. J Neurosci 2009; 29: 1615–25.

Fan J, Gandini MA, Zhang FX, Chen L, Souza IA, Zamponi GW. Down-regulation of T-type Cav3.2 channels by hyperpolarization-activated cyclic nucleotide-gated channel 1 (HCN1): evidence of a signaling complex. Channels 2017; 11: 434–43.

Fletcher CF, Lutz CM, O'Sullivan TN, Shaughnessy JD Jr, Hawkes R, Frankel WN, et al. Absence epilepsy in tottering mutant mice is associated with calcium channel defects. Cell 1996; 87: 607–17.

Glauser TA, Cnaan A, Shinnar S, Hirtz DG, Dlugos D, Masur D, et al. Ethosuximide, valproic acid, and lamotrigine in childhood absence epilepsy: initial monotherapy outcomes at 12 months. Epilepsia 2013; 54: 141–55.

Glauser TA, Cnaan A, Shinnar S, Hirtz DG, Dlugos D, Masur D, et al. Ethosuximide, valproic acid, and lamotrigine in childhood absence epilepsy. N Engl J Med 2010; 362: 790–9.

Gutierrez GJ, Marder E. Modulation of a single neuron has state-dependent actions on circuit dynamics. eNeuro 2014; 1. doi: 10.1523/ENEURO.0009-14.2014.

Hayashi S, Lewis P, Pevny L, McMahon AP. Efficient gene modulation in mouse epiblast using a Sox2Cre transgenic mouse strain. Mechanisms of development 2002; 119: S97–101.

Heron SE, Khosravani H, Varela D, Bladen C, Williams TC, Newman MR, et al. Extended spectrum of idiopathic generalized epilepsies associated with CACNA1H functional variants. Ann Neurol 2007; 62: 560–8.

Hess EJ, Wilson MC. Tottering and leaner mutations perturb transient developmental expression of tyrosine hydroxylase in embryologically distinct Purkinje cells. Neuron 1991; 6: 123–32.

Hou G, Smith AG, Zhang ZW. Lack of Intrinsic GABAergic Connections in the thalamic reticular nucleus of the mouse. J Neurosci 2016; 36: 7246–52.

Huang Z, Lujan R, Kadurin I, Uebele VN, Renger JJ, Dolphin AC, et al. Presynaptic HCN1 channels regulate Cav3.2 activity and neurotransmission at select cortical synapses. Nat Neurosci 2011; 14: 478–86.

Huang Z, Walker MC, Shah MM. Loss of dendritic HCN1 subunits enhances cortical excitability and epileptogenesis. J Neurosci 2009; 29: 10979–88.

Hubener M, Bonhoeffer T. Neuronal plasticity: beyond the critical period. Cell 2014; 159: 727–37.

Huguenard J. Current controversy: spikes, bursts, and synchrony in generalized absence epilepsy: unresolved questions regarding thalamocortical synchrony in absence epilepsy. Epilepsy Curr 2019; 19: 105–11.

Huntsman MM, Porcello DM, Homanics GE, DeLorey TM, Huguenard JR. Reciprocal inhibitory connections and network synchrony in the mammalian thalamus. Science 1999; 283: 541–3.

Joksovic PM, Bayliss DA, Todorovic SM. Different kinetic properties of two T-type Ca2 + currents of rat reticular thalamic neurones and their modulation by enflurane. J Physiol 2005; 566: 125–42.

Jun K, Piedras-Renteria ES, Smith SM, Wheeler DB, Lee SB, Lee TG, et al. Ablation of P/Q-type Ca(2 +) channel currents, altered synaptic transmission, and progressive ataxia in mice lacking the alpha(1A)-subunit. Proc Natl Acad Sci U S A 1999; 96: 15245–50.

Kakizawa S, Yamasaki M, Watanabe M, Kano M. Critical period for activity-dependent synapse elimination in developing cerebellum. J Neurosci 2000; 20: 4954–61.

Kano M, Nakayama H, Hashimoto K, Kitamura K, Sakimura K, Watanabe M. Calcium-dependent regulation of climbing fibre synapse elimination during postnatal cerebellar development. J Physiol 2013; 591: 3151–8.

Khosravani H, Altier C, Simms B, Hamming KS, Snutch TP, Mezeyova J, et al. Gating effects of mutations in the Cav3.2 T-type calcium channel associated with childhood absence epilepsy. J Biol Chem 2004; 279: 9681–4.

Khosravani H, Bladen C, Parker DB, Snutch TP, McRory JE, Zamponi GW. Effects of Cav3.2 channel mutations linked to idiopathic generalized epilepsy. Ann Neurol 2005; 57: 745–9.

Khosravani H, Zamponi GW. Voltage-gated calcium channels and idiopathic generalized epilepsies. Physiol Rev 2006; 86: 941–66.

Kim D, Song I, Keum S, Lee T, Jeong MJ, Kim SS, et al. Lack of the burst firing of thalamocortical relay neurons and resistance to absence seizures in mice lacking alpha(1G) T-type Ca(2 +) channels. Neuron 2001; 31: 35–45.

Lee SE, Lee J, Latchoumane C, Lee B, Oh SJ, Saud ZA, et al. Rebound burst firing in the reticular thalamus is not essential for pharmacological absence seizures in mice. Proc Natl Acad Sci U S A 2014; 111: 11828–33.

Ludwig A, Budde T, Stieber J, Moosmang S, Wahl C, Holthoff K, et al. Absence epilepsy and sinus dysrhythmia in mice lacking the pacemaker channel HCN2. EMBO J 2003; 22: 216–24.

Maheshwari A, Noebels JL. Monogenic models of absence epilepsy: windows into the complex balance between inhibition and excitation in thalamocortical microcircuits. Prog Brain Res 2014; 213: 223–52.

Mark MD, Maejima T, Kuckelsberg D, Yoo JW, Hyde RA, Shah V, et al. Delayed postnatal loss of P/Q-type calcium channels recapitulates the absence epilepsy, dyskinesia, and ataxia phenotypes of genomic Cacna1a mutations. J Neurosci 2011; 31: 4311–26.

McCafferty C, David F, Venzi M, Lorincz ML, Delicata F, Atherton Z, et al. Cortical drive and thalamic feed-forward inhibition control thalamic output synchrony during absence seizures. Nat Neurosci 2018; 21: 744–56.

McCormick DA, Contreras D. On the cellular and network bases of epileptic seizures. Ann Rev Physiol 2001; 63: 815–46.

Meeren HK, Pijn JP, Van Luijtelaar EL, Coenen AM, Lopes da Silva FH. Cortical focus drives widespread corticothalamic networks during spontaneous absence seizures in rats. J Neurosci 2002; 22: 1480–95.

Miao Q, Yao L, Rasch MJ, Ye Q, Li X, Zhang X. Selective maturation of temporal dynamics of intracortical excitatory transmission at the critical period onset. Cell Rep 2016; 16: 1677–89.

Midorikawa M, Okamoto Y, Sakaba T. Developmental changes in Ca2 + channel subtypes regulating endocytosis at the calyx of Held. J Physiol 2014; 592: 3495–510.

Nishitani A, Kunisawa N, Sugimura T, Sato K, Yoshida Y, Suzuki T, et al. Loss of HCN1 subunits causes absence epilepsy in rats. Brain Res 2019; 1706: 209–17.

Noebels JL, Sidman RL. Inherited epilepsy: spike-wave and focal motor seizures in the mutant mouse tottering. Science 1979; 204: 1334–6.

Notomi T, Shigemoto R. Immunohistochemical localization of Ih channel subunits, HCN1-4, in the rat brain. The J Comp Neurol 2004; 471: 241–76.

O'Leary T, Williams AH, Franci A, Marder E. Cell types, network homeostasis, and pathological compensation from a biologically plausible ion channel expression model. Neuron 2014; 82: 809–21.

Pellegrini C, Lecci S, Luthi A, Astori S. Suppression of sleep spindle rhythmogenesis in mice with deletion of CaV3.2 and CaV3.3 T-type Ca(2 +) channels. Sleep 2016; 39: 875–85.

Peloquin JB, Khosravani H, Barr W, Bladen C, Evans R, Mezeyova J, et al. Functional analysis of Ca3.2 T-type calcium channel mutations linked to childhood absence epilepsy. Epilepsia 2006; 47: 655–8.

Polack PO, Guillemain I, Hu E, Deransart C, Depaulis A, Charpier S. Deep layer somatosensory cortical neurons initiate spike-and-wave discharges in a genetic model of absence seizures. J Neurosci 2007; 27: 6590–9.

Proft J, Rzhepetskyy Y, Lazniewska J, Zhang FX, Cain SM, Snutch TP, et al. The Cacna1h mutation in the GAERS model of absence epilepsy enhances T-type Ca(2 +) currents by altering calnexin-dependent trafficking of Cav3.2 channels. Sci Rep 2017; 7: 11513.

Rajakulendran S, Graves TD, Labrum RW, Kotzadimitriou D, Eunson L, Davis MB, et al. Genetic and functional characterisation of the P/Q calcium channel in episodic ataxia with epilepsy. J Physiol 2010; 588: 1905–13.

Santoro B, Chen S, Luthi A, Pavlidis P, Shumyatsky GP, Tibbs GR, et al. Molecular and functional heterogeneity of hyperpolarization-activated pacemaker channels in the mouse CNS. J Neurosci 2000; 20: 5264–75.

Shipe WD, Barrow JC, Yang ZQ, Lindsley CW, Yang FV, Schlegel KA, et al. Design, synthesis, and evaluation of a novel 4-aminomethyl-4-fluoropiperidine as a T-type Ca2 + channel antagonist. J Med Chem 2008; 51: 3692–5.

Song I, Kim D, Choi S, Sun M, Kim Y, Shin HS. Role of the alpha1G T-type calcium channel in spontaneous absence seizures in mutant mice. J Neurosci 2004; 24: 5249–57.

Sun YJ, Wu GK, Liu BH, Li P, Zhou M, Xiao Z, et al. Fine-tuning of pre-balanced excitation and inhibition during auditory cortical development. Nature 2010; 465: 927–31.

Talley EM, Cribbs LL, Lee JH, Daud A, Perez-Reyes E, Bayliss DA. Differential distribution of three members of a gene family encoding low voltage-activated (T-type) calcium channels. J Neurosci 1999; 19: 1895–911.

Tenney JR, Fujiwara H, Horn PS, Vannest J, Xiang J, Glauser TA, et al. Low- and high-frequency oscillations reveal distinct absence seizure networks. Ann Neurol 2014; 76: 558–67.

Toulmin H, Beckmann CF, O'Muircheartaigh J, Ball G, Nongena P, Makropoulos A, et al. Specialization and integration of functional thalamocortical connectivity in the human infant. Proc Natl Acad Sci U S A 2015; 112: 6485–90.

Tsakiridou E, Bertollini L, de Curtis M, Avanzini G, Pape HC. Selective increase in T-type calcium conductance of reticular thalamic neurons in a rat model of absence epilepsy. J Neurosci 1995; 15: 3110–7.

Wakamori M, Yamazaki K, Matsunodaira H, Teramoto T, Tanaka I, Niidome T, et al. Single tottering mutations responsible for the neuropathic phenotype of the P-type calcium channel. J Biol Chem 1998; 273: 34857–67.

Wang G, Bochorishvili G, Chen Y, Salvati KA, Zhang P, Dubel SJ, et al. CaV3.2 calcium channels control NMDA receptor-mediated transmission: a new mechanism for absence epilepsy. Genes Dev 2015; 29: 1535–51.

Yoshimura Y, Inaba M, Yamada K, Kurotani T, Begum T, Reza F, et al. Involvement of T-type Ca2+ channels in the potentiation of synaptic and visual responses during the critical period in rat visual cortex. Eur J Neurosci 2008; 28: 730–43.

Zhang Y, Mori M, Burgess DL, Noebels JL. Mutations in high-voltage-activated calcium channel genes stimulate low-voltage-activated currents in mouse thalamic relay neurons. J Neurosci 2002; 22: 6362–71.

Zhang Y, Vilaythong AP, Yoshor D, Noebels JL. Elevated thalamic low-voltage-activated currents precede the onset of absence epilepsy in the SNAP25-deficient mouse mutant coloboma. J Neurosci 2004; 24: 5239–48.